Atomic Force Microscopy 를 이용한 수산칼슘 결정 성장의 실시간 관찰

정태성, Xiaoxia Sheng[1], 김우식*[2], Jeffrey A. Wesson[3], Michael D. Ward[1], 최창균
서울대학교 응용화학부,
[1]미네소타 대학교 화학 및 재료공학과,
[2]경희대학교 화학공학과,
[3]위스콘신 의과대학
(wskim@khu.ac.kr*)

Real-time Atomic Force Microscopy Investigation of Calcium Oxalate Crystal Growth

TaeSung Jung, Xiaoxia Sheng[1], WooSik Kim*[2], Jeffrey A. Wesson[3],
Michael D. Ward[1], ChangKyun Choi
School of Chemical Engineering, Seoul National University,
[1]Department of Chemical Engineering and Materials Science, University of Minnesota,
[2]Department of Chemical Engineering, Kyunghee University,
[3]Department of Veterans Affairs Medical Center, Medical College of Wisconsin
(wskim@khu.ac.kr*)

Introduction

The formation of calcium oxalate monohydrate (COM), which is regulated by urinary (macro)molecules, is an important issue in kidney stone formation.[1,2] These organic (macro)molecules in urine can act as inhibitors of the stone formation but the microscopic origin underlying these phenomena remains ambiguous. In this study, atomic force microscope (AFM) enabling direct imaging of nucleation and crystal growth events at the microscopic level[3-5] is applied to visualize the COM crystal surface and to measure the growth rate of steps/pits in three different faces. Using *in situ* AFM, the inhibiting effect of the urinary protein-like macromolecules: poly(acrylate), poly(aspartate), and poly(glutamate), is investigated along specific crystallographic directions. These face-specific inhibitions observed by AFM can guide the understanding the local phenomena that govern calcium oxalate crystallization and the nature of protein-crystal interactions.

Experimental

Calcium chloride dihydrate, sodium oxalate, sodium polyacrylate (polyAA, 5.1 kDa), oxalic acid (Aldrich), sodium poly-L-aspartate (polyD, 8.3 kDa), sodium poly-L-glutamate (polyE, 6.63 kDa) (Sigma) were used without further purification. COM crystals were synthesized according to literature procedures.[6,7] The COM crystals having large {010} surface was prepared by adding 15 mM $CaCl_2$ and 15 mM $Na_2C_2O_4$ into a vessel containing 500 mL deionized water, which was well stirred at 75±5ºC.[6] When the solution became turbid, the reactant solutions were changed to 4 mM stock solutions (37 mL/hr). The crystallization was terminated after 10 hours and the final volume of product solutions was 800 mL. Most of the obtained apparently were uniform single crystals with a large surface (10-30 μm) enclosed with six edges (Figure 1a). The other COM crystals with {12-1} and {100} dominant surfaces were obtained by slow evaporation of acidic saturated CaOx solution.[7] After vigorously mixing equi-volume of 100 mM $CaCl_2$ and 100 mM $H_2C_2O_4$ for 10 minutes, the abruptly formed particles were removed by membrane filtration. The filtered CaOx saturated solution (100 mL) was evaporated at room temperature until the volume became 20 mL. The formed crystals had various shapes such as twins but mostly large (10-30 μm length) xiphoid face (Figure 1b). In a few of upright crystals, small (5-15 μm length) diamond shaped surface was observed (Figure 1c). Each of the crystals was separated from the solution with a membrane filter (polycarbonate, 10 μm pore) and transferred to an AFM specimen disc coated with UV curable optical cement.

In situ Atomic force microscopy (AFM) was performed in contact mode using a Nanoscope E Multimode system (Digital Instruments), a glass liquid cell, a scanner with a maximum 15 μm scan range, and a 200 μm Si_3N_4 cantilever tip with a force constant of 0.06 N/m. All data were acquired in deflection and height mode with resolution of 256 and set point of 0 and a high scan rate of 10.2 Hz to overcome possibly fast crystal growth rate. Typical scan size ranged from 2×2 to 4×4 m^2, which corresponded to probe movement rate of 40.8 to 81.6 μm/s. Working solutions were injected by a syringe via Teflon tube and allowed to stand without any refreshment at room temperature. All data were collected within 20 minutes after the injection of the working solution. The morphology of the crystals was obtained with a Leitz ERGOLUX optical microscope and a Jeol JSM-5600 scanning electron microscope.

Results and Discussion

To define the crystal face, the crystal system reported by Tazzoli and Domeneghetti[8] ($P2_1/c$, a = 6.290 Å, b = 14.5803 Å, c = 10.226 Å, β = 109.46°) was used for convenience. Each of the crystal face can be determined on the basis of the dihedral angles. The assignment of the faces and the crystallographic orientation is shown in Figure 1d-f. When the surface of the crystals shown in Figure 1a was imaged in saturated CaOx solution, the lattice parameter of the unit cell was 7.0 Å, 9.56 Å, and 109.4° in agreement with the lattice parameters, a, c, and β (Figure 2a) and the step height was 14.7 Å, which is close to d_{010} (Figure 2b). The (12-1) face having unit vectors along [-210] and [012] directions was verified in the same manner (Figure 2c, d). Due to the roughness of the (100) face, two-dimensional periodicity was difficult to discern in its real space lattice images. Fourier transforms of the AFM data, however, revealed one strong frequency component as one-dimensional features oriented along the [021] direction, at an angle of 35.2° with respect the *c*-axis (Figure 2e). Larger scan areas revealed narrow terraces aligned along the *c*-axis, separated by steps with heights of 6.3 Å, essentially identical to d_{100} = 5.93 Å (Figure 2f). These lattice images and step height measurements corroborate the assignment of the (010), (12-1), and (100) faces deduced from the crystal habit analysis, providing the unambiguous determination of the crystal orientation that is necessary for reliable characterization of crystal growth modes.[9]

Exposure of the crystals to highly supersaturated CaOx solutions dramatically produced growth hillocks, whose shapes were different from each face. The edges of each growth hillocks identically oriented along each bulk crystal. The (010) surface formed four-sided parallelogram hillocks with well-defined step edges: shorter {12-1} and longer {021} (Figure 3a). When the concentration was lowered to 0.10 mM CaOx, just below the equilibrium concentration, the {100} face dissolved and well-defined etch pits were formed and the crystal faces of the edges were oriented in the same direction (Figure 3b). The growth hillocks on (12-1) face with 6 edges composed of (0-2-1), (1-2-1), (100), (010), and (02-1) formed under near equilibrium concentration and had shapes that mimicked the xiphoid habit of the bulk crystal (Figure 3c). The xiphoid habit of etch pits on (12-1) face showed the same edge faces but oriented in opposite direction (Figure 3d). The (100) face exhibited large tear-shaped hillocks emanating from a single point source at one end of the bulk crystal and had (021), (0-21), (12-1), (1-2-1) steps (Figure 3e). In undersaturated solution, the {100} face dissolved and well-defined triangular pits were formed on the crystal surface (Figure 3f). The triangular etch pits and growth hillocks on (100) were oriented in opposite directions along the *c* axis.

The growth of tear-shaped spiral hillocks on the (100) face were changed by the macromolecule additives, polyAA, polyD, and polyE (*e.g.*, rough steps and narrow terraces) and the inhibition effect increased as increasing the polymer concentration. Data acquired on the (100) face, $v_{[001]}$, clearly revealed that polyAA was the most potent inhibitor of growth and that polyD was more effective than polyE (Figure 4a). Unlike these anionic polymers, cationic polymers: polyH, polyK, and polyR, disturbed crystal growth only at higher concentration (ca 100 μg/mL). The effect of macromoleculat binding to the (010) hillocks is even more apparent from the complete loss of hillock features when the macromolecule concentrations exceeded to a critical point. For example, the (010) hillocks became unrecognizable by addition of 2.5 μg/mL polyD (Figure 5) PolyAA was a strong inhibitor of growth

on steps of the (010) hillocks as well but the effectiveness of polyE and polyD were inverted compared with the (010) hillocks, with polyE inhibiting step motion more strongly. Therefore, it is clear that the effect of polyE and polyD on the (021) step velocity depends upon whether this step plane intersects with the (010) or (100) plane.

The explored polymers have carboxylate groups in side chain but differ with respect to the number of methylene groups in the side chain. PolyAA with the shortest chain and different backbone revealed the strongest inhibition effect on both faces. The competing effect between polyD and polyE on (100) and (010) faces is ascribed to different macromolecular binding to the crystal planes of the step site, which can be affected by steric and side chain conformation. Interestingly, the stronger binding of polyE to {010} surface than polyD were consistent with the trends in pit filling experiment in our previous report.[4] Unlike (100) and (010) face, two dimensional islands were investigated in (12-1) face instead of spiral growth hillocks, which were less dominantly formed. The spreading rate revealed polyAA is the most effective inhibitor.

Conclusions

* The calcium oxalate monohydrate (COM) crystals having three different faces were synthesized and their growth was investigated in microscopic level using real-time AFM. The lattice imaging of unit cell on each surface and step height of larger scan area enable to identify crystallographic orientation and crystal faces: {010}, {12-1}, and {100}.
* The growth mode of the specific steps in spiral hillocks and etch pits was changed by urinary protein-like synthetic macromolecules: polyAA, polyD, and polyE. The inhibition effect of polyD and polyE competed on {010} and {100}, while polyAA most effectively stopped crystal growth and destructed the growth hillocks on every face.
* The macromolecules explored here contain anionic side chains and the inhibition profiles of all three macromolecules clearly reveal the importance of side chain structure with respect to binding to the crystal surfaces.

References

1. Mandel, N. S. and Mandel, G. S.: *J. Urol.*, **142**, 1516(1989).
2. Shiraga, H., Min, W., Van Dusen, W. J., Clayman, M. D., Miner, D., Terrell, C. H., Sherbotie, J. R., Foreman, J. W., Przysiecki, C., Neilson, E. G., and Hoyer, J. R.: *Proc. Natl. Acad. Sci. USA*, **89**, 426(1992).
3. Sheng, X. X., Ward, M. D., and Wesson, J. A.: *J. Am. Chem. Soc.*, **125**, 2854(2003).
4. Guo, S. W., Ward, M. D., and Wesson, J. A.: *Langmuir*, **18**, 4284(2002).
5. Orme, C. A., Noy, A., Wierzbicki, A., McBride, M. T., Grantham, M., Teng, H. H., Dove, P. M., and De Yoreo, J. J.: *Nature*, **411**, 775(2001).
6. Millan, A.: *Cryst. Growth Des.*, **1**, 245(2001).
7. Cody, A. M. and Horner, H. T.: *Scanning Electron Microsc.*, **3**, 1451(1984).
8. Tazzoli, V. and Domeneghetti, C.: *Am. Mineral.*, **65**, 327(1980).
9. Ward, M. D.: *Chem. Rev.*, **101**, 1697(2001).

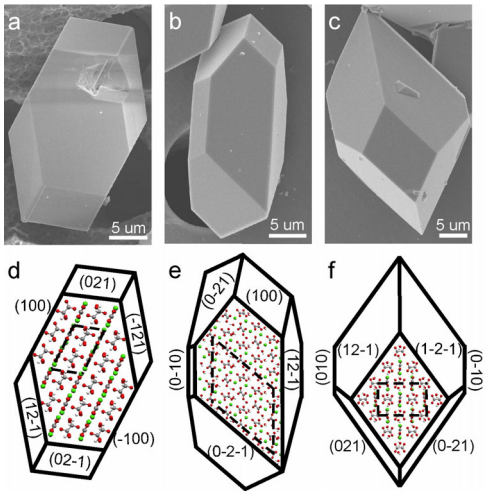

Figure 1. SEM images of COM crystals with their (010), (12-1), and (100) faces (top) and their schematic representations (bottom).

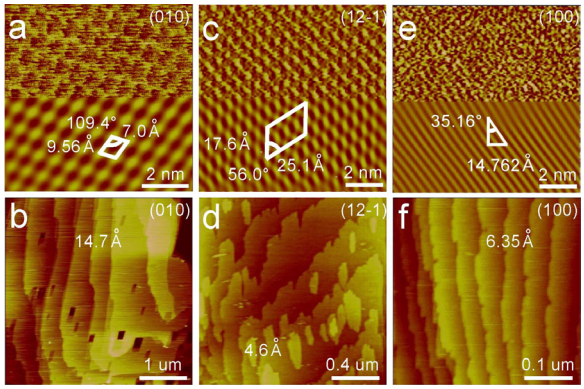

Figure 2. AFM lattice images of the (010), (12-1), and (100) faces of COM single crystals (top) and corresponding images of larger areas (bottom).

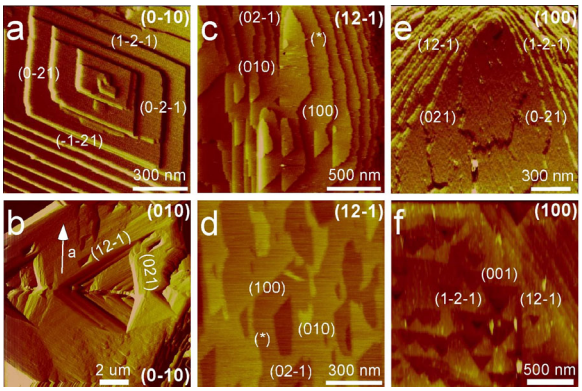

Figure 3. AFM images of growth hillocks and etch pits. Panels (a), (c), (e): Growth hillocks on the (0-10), (12-1), and (100) faces. Panels (b), (d), (f): Etch pits on the three faces.

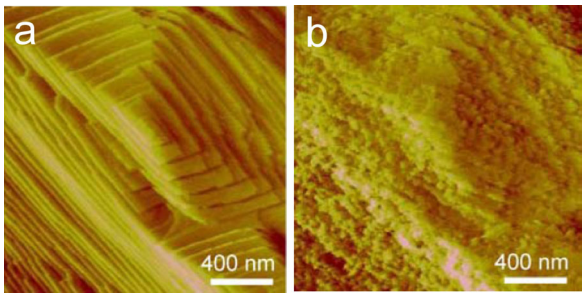

Figure 5. AFM images of the (010) hillocks: (a) before addition of polyD and (b) immediately (< 1 minute) following addition of 2.5 μg/mL polyD.

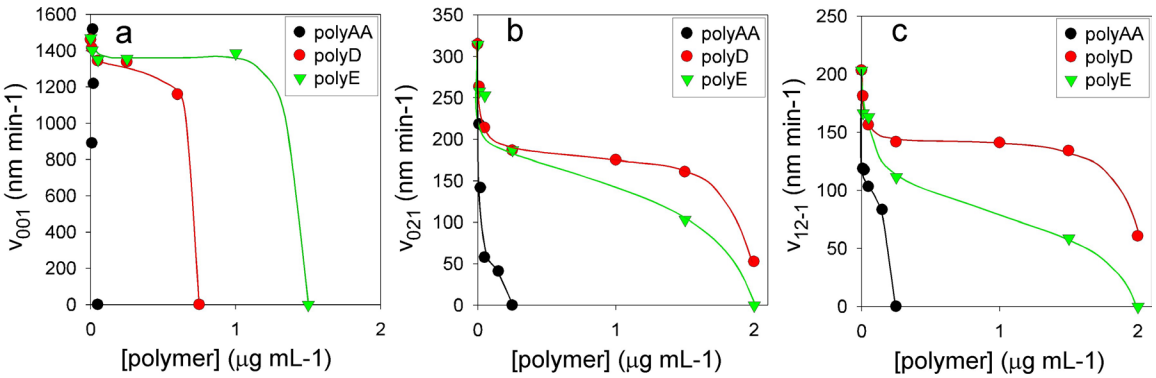

Figure 4. The inhibition of (a) the step velocity along the [001] direction and (b) (021) and (c) (12-1) step velocities in the presence of polyAA, polyD, and polyE.